Korean J. Chem. Eng., **16**(1), 104-110 (1999)

MODELING OF THE MONOMER ROLE AND THE COALESCENCE LIMITATION IN PRIMARY PARTICLE GROWTH

Young-Soo Han, Kun-Moo Lee, Sun-Geon Kim†, Hee-Dong Jang and Kyun Young Park*****

Department of Chemical Engineering, Chung Ang University, 221 Huksuk-Dong, Dongjak-Ku, Seoul 156-756, Korea
*Mineral Utilization & Material Development Division, Korea Institute of Geology, Mining & Materials, 30 Kajung Dong, Yusong Ku, Taejon 305-350, Korea
**Department of Chemical Engineering, Kongju University, 182 Shinkwangdong, Kongju, Chungnam 314-701, Korea
(Received 5 August 1998 • accepted 7 October 1998)

Abstract – The 'general dynamic' equation (GDE) has been numerically solved to simulate the growth of ultrafine particles (UFPs) in a tubular aerosol reactor, approximating the particle size distribution by a lognormal function. The GDE includes all the terms describing diffusion, thermophoresis, nucleation, condensation and coagulation. We have also considered the efficiency of liquid-like coagulation to primary particles. The data calculated from our model were compared with those from the previous model and also with some experimental results from a TiO_2 UFP generator. The condensation term, which we split from a single coagulation term in the previous model, well described the monomer contribution to the particle growth. Introduction of one adjustable parameter, the efficiency of coagulation, was successful in limiting the growth of primary particles and fit the experimental data.

Key words: Ultrafine Particles, Growth, Simulation, General Dynamic Equation, Moment Transformation, Coagulation Efficiency, Condensation

INTRODUCTION

The general dynamic equation has been used for simulating the growth of ultrafine particles in a tubular aerosol reactor. Approximating the particle size distribution by a lognormal function, the GDE, the integrodifferential equation, is transformed into three ordinary differential equations [Pratsinis and Kim, 1989]. The ordinary differential equations are solved, along with the mass balances of reactant (precursor) and monomer (product) in known temperature and velocity fields. The previous model, in which coagulation was included as the only growth term, however, had some drawbacks. In the model, monomers were considered as critical nuclei and their size was used as a lower limit of the integral in moment transformation. However, the model would not reasonably predict particle behavior in the early stage of growth when the monomer concentration is high compared to that of larger particles so the size distribution hardly follows the lognormal function [Landgrebe and Pratsinis, 1990]. On the other hand, primary particles in the coagulation-only model grow without the limit of their size. In fact, the primary particles can grow only to a certain size that is determined by the sintering rate of colliding particles. The model also could not explain some experimental results showing that the primary particle size decreased with the reactor temperature.

We revived the condensation term in its original form of the GDE in order to overcome the drawbacks of the previous model. In this study, the critical nuclei were assumed dimers and, therefore, the rate of nucleation was expressed as the rate of dimer formation. Our model was compared with the previous one and also with the experimental data obtained from the aerosol reactor which produced the TiO_2 particles from the oxidation of $TiCl_4$ [Chang et al., 1995]. We also introduced one adjustable parameter, the efficiency of coagulation, in order to limit the primary particle growth.

†To whom correspondence should be addressed.
E-mail : sgkim@ripe.chungang.ac.kr

MODELING AND SIMULATION

1. Fundamental Equations

The equations necessary to simulate the particle behavior in a tubular aerosol reactor include the continuity equation, momentum (Navier-Stokes equation) and energy balances in gas phase, mass balances for precursor vapor and product monomer, and general dynamic equation (GDE) of the particles in the gas.

Here, we assumed that the chemical reaction and particle behavior do not influence the velocity and temperature profiles of the carrier gas. The profiles were then found by solving simultaneously the continuity, Navier-Stokes and energy balance equations all in steady-state forms. When u, v, and T are the axial, radial velocities and temperature of the carrier gas, respectively, the boundary conditions are given as follows:

$$u = 0 \text{ and } T = T_w \text{ at } r = R \text{ and } 0 < z \leq z_T \quad (1)$$

$$u = u_0,\ v = 0 \text{ and } T = T_0 \text{ at } z = 0 \quad (2)$$

where r and z are the radial and axial coordinates, respectively, and R and z_T are the radius and length of the reactor. T_w u_0 and T_0 are the temperature of the reactor wall, velocity and temperature of the carrier gas at the reactor inlet, respectively. The boundary condition at the exit of the reactor is given by the condition that mass flow rate of the carrier gas there is equal to that

at the reactor inlet. Then the three equations were solved with TEACH code. The conversion tests were made whether the normalized residual-source sum is sufficiently small (0.005).

The precursor vapor mass balance inside the reactor tube is:

$$\nabla \cdot (\rho \vec{V} C) = \nabla \cdot (\rho D \nabla C) - RXN \tag{3}$$

where ρ and $\vec{V}$ are the density and velocity of the carrier gas, and D and C are the diffusion coefficient and mass concentration of the precursor vapor component. The second RHS term represents the reaction rate for the precursor.

The monomer mass balance is:

$$\nabla \cdot (\rho \vec{V} C_1) = \nabla \cdot (\rho D_1 \nabla C_1) + RXN - \int_{x^*}^{\infty} x \nu(x) \delta(x - x^*) dx - \int_{x^*}^{\infty} \phi(x, C_1) n(x, \vec{r})\, dx \tag{4}$$

The third and fourth RHS terms represent consumption rates of the monomers due to nucleation and condensation, respectively. In the equation C_1 and D_1 are the mass concentration and the diffusion coefficient of monomer vapor, respectively. $\nu(x)$ in the third RHS term accounts for the formation rate of the nuclei with mass x and x^* is the mass of the critical nuclei, the dimer in this study. $\phi(x, C_1)$ represents the growth rate of the particles with mass x and $n(x, \vec{r})$ represents the size distribution function of particles with mass x and at the location $\vec{r}$.

The general dynamic equation of the particles [Brock, 1983] is:

$$\nabla \cdot [\rho \vec{v} n(x, \vec{r})] = \nabla \cdot [\rho D_p \nabla n(x, \vec{r}) + \vec{v}_T n(x, \vec{r})] + \nu(x) \delta(x - x^*) dx - \frac{\partial}{\partial x}[\phi(x, C_1) n(x, \vec{r})] + \frac{1}{2} \int_{x^*}^{x} \eta b(x - x', x') n(x - x', \vec{r}) dx' - n(x, \vec{r}) \int_{x^*}^{\infty} \eta b(x', x) n(x', \vec{r}) dx' \tag{5}$$

The first RHS term accounts for the particle transport by Brownian diffusion and drift flow by external forces, where D_p and v_T are the diffusion coefficient and drift velocity of particles, respectively. The second and third RHS terms represent the rates of nucleation and condensation, respectively. The fourth and fifth RHS terms account for the rate of coagulation, where b(x, x') represents the coefficient of coagulation between two particles with the masses, x and x', respectively. η in the terms represents the efficiency of coagulation, the occurrence probability of the liquid-like coagulation between the two colliding particles.

The initial conditions for the equations above are:

$$C = C_0,\ C_1 = 0 \text{ and } n(x) = 0 (\text{for all x}) \text{ at } z = 0 \tag{6}$$

$$\frac{\partial C}{\partial z} = \frac{\partial C_1}{\partial z} = \frac{\partial n(x)}{\partial z} (\text{for all x}) = 0 \quad \text{at } r = 0 \text{ and for } 0 \le z \le z_T \tag{7}$$

$$\frac{\partial C}{\partial z} = \frac{\partial C_1}{\partial z} = 0 \text{ and } n(x) = 0 (\text{for all x}) \quad \text{at } r = R \text{ and for } 0 \le z \le z_T \tag{8}$$

2. Expressions of Rates of Nucleation and Condensation

In general the solid materials composing the particles have very low vapor pressures at the temperature of the reactor where they are produced. Therefore, the vapor molecules (monomer), as they are produced by the reaction, show very high supersaturation, which results in very small size of nuclei and very high rate of nucleation. The size of the critical nuclei calculated from the classical nucleation theory is, usually, less than that of single molecule. Kim and Pratsinis [1989], therefore, assumed a nucleus as a molecule (x_1). Then, the nucleation term in GDE is represented by the monomer formation, which is, in turn, the rate of reaction. The condensation term disappeared in their model, since the condensation of monomers on the particles was included in the coagulation as far as the monomers were considered as the smallest particles. Therefore, the only growth term in their model was the coagulation term. However, the condensation and coagulation must be differentiated in the growth simulation for the solid-phase particles. The coagulation between such particles is completed only after complete sintering occurs and the identities of the two particles are lost. This coagulation process needs some time, which may be longer than the residence time of the particles in the reactor. On the other hand, the condensation of monomers can occur instantaneously due to its high mobility in the particle. The assumption of lognormal distribution including monomers also has some problem. The monomer number concentration is high at least in the inlet of the reactor, where the reaction occurs vigorously. However, in the lognormal distribution, the concentration of the monomers, the smallest particles, becomes very low, just as particles grow, due to the characteristics of the distribution. In this study, a nucleus was assumed as a dimer (x_2) [Kim and Brock, 1987], so that we can treat the condensation and coagulation independently to make up for the drawbacks of the previous model.

The rate of nucleation is then expressed as the collision rate of two monomers:

$$\nu(x) \delta(x - x^*) = b(x_1, x_1) C_1^2 / x_1^2 \tag{9}$$

Here, x_1 and x^* are the mass of monomers and dimers, respectively, and $b(x_1, x_1)$ is the coefficient of the collision between two monomers and expressed in free molecule regime as:

$$b(x_1, x_1) = \left(\frac{3}{4\pi}\right)^{1/6} (6kT)^{1/2} \rho_p^{-2/3} 4\sqrt{2}\, x_1^{1/6} \tag{10}$$

In the equation above, k is the Boltzmann constant, T the temperature of the carrier gas, ρ_p the density of the particles and x_1 is the mass of monomer.

On the other hand, the rate of particle growth by condensation of monomer is [Brock, 1983]:

$$\phi(x, C_1) = \pi \left(\frac{3}{4\pi\rho_p}\right)^{2/3} x_1^{2/3} \left(\frac{8kT}{\pi x_1}\right)^{1/2} C_1 \left(\frac{1 + Kn}{1 + 1.71Kn + 1.333Kn^2}\right) \tag{11}$$

Here, Kn accounts for the Knudsen number, expressed as λ/d_p, where λ is the mean free path of the carrier gas molecules.

3. Experiment and Simulation

In this study the target particle was chosen as TiO_2 prepared by the reaction between $TiCl_4$ and O_2. The experimental apparatus and results were given elsewhere [Chang et al., 1995]. In brief, the reactor made of quartz tube was a tubular reactor with a diameter of 0.03 m and a length of 0.75 m. The reac-

tants [$TiCl_4$ vaporized and O_2] and inert carrier gas (N_2) were introduced in well-mixed state at a predetermined preheating temperature. The reactor was heated externally in an electrical furnace. The $TiCl_4$ concentration in the inert gas, preheating temperature, furnace (reactor) temperature, and oxygen and carrier gas flow rates were chosen as process variables. Table 1 shows the process variables they used.

The rate of the oxidation of $TiCl_4$ is expressed as first order with respect to $TiCl_4$ and zeroth order to oxygen, and its rate constant is [Akhtar et al., 1991]:

$$k(T) = 8.29 \times 10^4 s^{-1} \exp(-8.88 \times 10^4 / 8.314T(K)) \quad (12)$$

The size distribution function is transformed to k-th moment, M_k by integration [Lee et al., 1984]:

$$M_k(\vec{r}) = \int_{x^*}^{\infty} x^k n(x, \vec{r})\, dx \quad (13)$$

By this definition, all the terms in Eq. (5) can be transformed to form an ordinary equation. Three ordinary differential equations are obtained for k=0, 1 and 2, respectively. In order to include the condensation term in the transformation, we expanded the last bracket in Eq. (11) in terms of the inverse of the Knudsen number (1/Kn) by Taylor series:

$$\frac{1+Kn}{1+1.71Kn+1.333Kn^2} \cong 1.000528 - 0.371706\left(\frac{1}{Kn}\right) + 0.029874\left(\frac{1}{Kn}\right)^2$$

Standard error in the approximation above was within 0.0015. Fractional moments in transformed equations were expressed in terms of the zeroth, first and second moments by assuming the size distribution of particles lognormal [Kim and Pratsinis, 1989].

Now we have five equations including the mass balance equations for the precursor vapor, $TiCl_4$ and the monomer, TiO_2, respectively, and three equations transformed from GDE for k=0, 1 and 2. They were solved simultaneously with the initial-value problem solver, LSODE for each set of the experimental conditions (Table 1). For each set, two solutions were obtained: one for perfect coagulation (η=1), designated by Model CC, and the other for limited coagulation (η<1) designated by Model CC-L. In the latter case, the efficiency of coagulation, η, was chosen as 0.1 by adjusting to get the same particle diameter with the experiment under the reference condition given in Table 1. The value chosen implies that only 10 % of the collisions are effective for growth as primary particles. It was fixed for the calculations for other sets of the conditions. We then compared our new models (Models CC and CC-L) with the previous coagulation-only model (Model C) and the experimental data on the TiO_2 UFPs [Chang et al., 1995].

Table 1. Variation in process variables

Process variables	Values
Reaction temperature (K)	1173*, 1273, 1373
Inlet $TiCl_4$ concentration (mol %)	0.05, 0.1, 0.5*
Inlet O_2 concentration (mol %)	12.4, 37.3, 49.75*
Carrier gas flow rate ($\times 10^{-5}$ m^3/s)	5.00, 6.67*, 8.34

*reference condition.

RESULTS AND DISCUSSION

1. The Role of Monomers and Comparisons of the Models

Fig. 1 shows the mass concentrations of the precursor ($TiCl_4$), monomer (TiO_2), and particles along the reactor axis in Models CC and CC-L in logarithmic scale in order to investigate the early-stage particle formation. Both models have little difference in the values shown in the figure. We see that the concentration of TiO_2 monomers increases up to 10^{-4} m from the reactor inlet and then decreases while the total mass concentration of the particles (here, those greater than the dimer) increases continuously surpassing that of the monomers around the point of the maximum monomer concentration.

Fig. 2 shows the axial distributions of the zeroth moments (total number concentration of the particles) calculated with various models. It is no wonder that the concentration of Model CC is lower than that of Model C, since the monomer con-

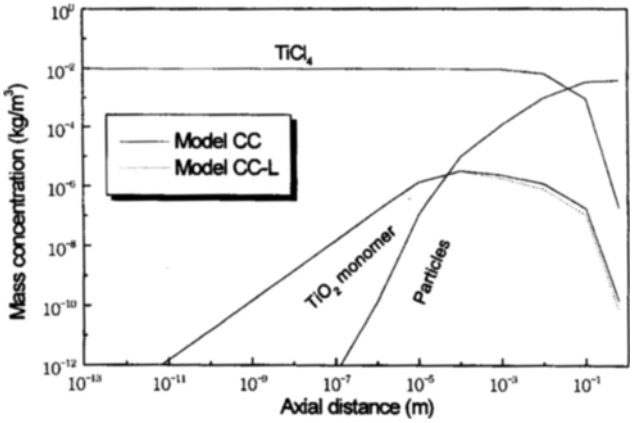

Fig. 1. Axial distribution of mass concentrations of $TiCl_4$, TiO_2 monomer and the first moment of the particles from Models CC and CC-L.
(T_{in}=1,173 K, T_w=1,173 K, $TiCl_4$=0.5 mole %, O_2=49.75 mole %, carrier gas flow rate=4×10^{-3} m^3/min)

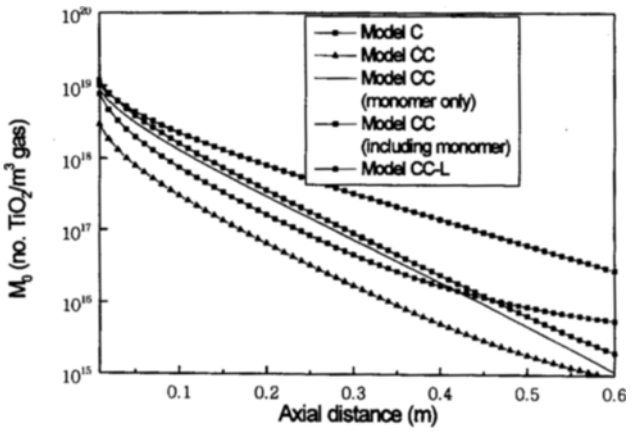

Fig. 2. Axial distribution of number concentrations of the particles and monomers for various models.
(T_{in}=1,173 K, T_w=1,173 K, $TiCl_4$=0.5 mole %, O_2=49.75 mole %, carrier gas flow rate=4×10^{-3} m^3/min)

centration is excluded in the former. However, even though the number concentration of the monomers is added to that of the particles, the total concentration is still lower than the particle concentration of Model C, as shown in the figure. In addition, in Model CC, the monomer concentration is always higher than the total particle concentration. This is not true in Model C, as described before. Therefore, the Model C, which regards the monomer concentration as very low, cannot well simulate the whole particle growth. The monomers have much higher mobility for particle growth than larger particles. They condense onto the surface of the existing particles much faster than the particles coagulate with each other. Therefore, the total number concentration of the particles plus monomers in Model CC decreases faster than that of the particles in Model C.

As shown in the figure, the particle concentrations obtained in Model CC-L are between those of Models C and CC, since the coagulation rate, the rate of particle number decrease, is limited by the efficiency,.

The axial distributions of the total mass concentrations of the particles are shown in Fig. 3. In Models CC and CC-L the monomer mass concentration is negligible after passing a very short distance from the reactor inlet, as shown in Fig. 1, even though their number concentrations remain relatively high. The three models, therefore, have no appreciable difference in mass concentration. Fig. 4 shows the axial distribution of the second moments of the particle size distribution, which is related to the dispersion of particle sizes. Model C has the highest values of the three models and Model CC-L the lowest. Since coagulation is known to increase the particle polydispersity [Hinds, 1982], it is clear that the split of condensation from the coagulation-only growth suppresses the increase in the second moment, and the limited coagulation model further suppresses the polydispersity of the distribution. In Fig. 5, the average diameters of the particles are plotted along the reactor axis. Model C, which has highest number concentration of particles for almost the same mass source of particles, results in the smallest particles. The particles grow in similar fashion in models C and CC, while the rate of the growth in model CC-L is more or

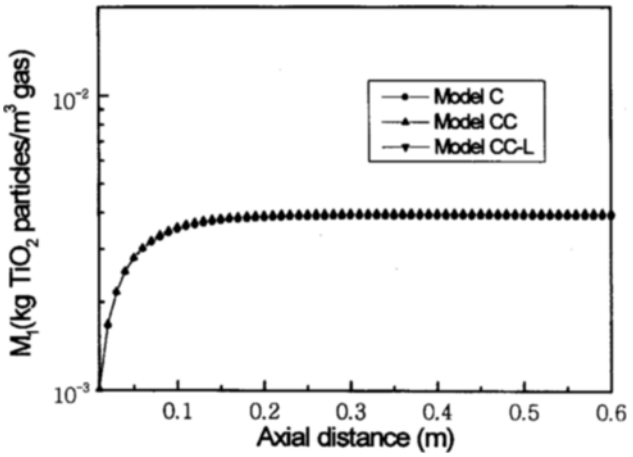

Fig. 3. Axial distribution of mass concentrations of the particles for various models.
(T_{in}=1,173 K, T_w=1,173 K, $TiCl_4$=0.5 mole %, O_2=49.75 mole %, carrier gas flow rate=4×10^{-3} m^3/min)

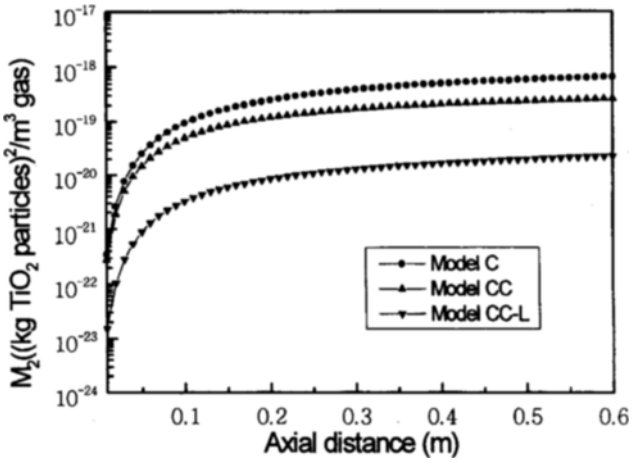

Fig. 4. Axial distribution of the second moments of the particle size distribution for various models.
(T_{in}=1,173 K, T_w=1,173 K, $TiCl_4$=0.5 mole %, O_2=49.75 mole %, carrier gas flow rate=4×10^{-3} m^3/min)

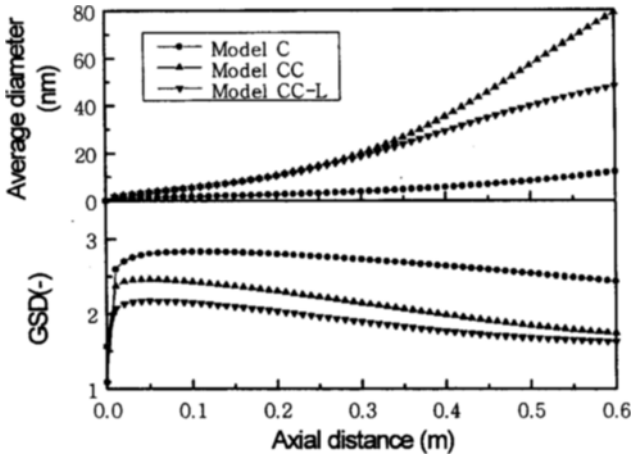

Fig. 5. Axial distribution of the average diameters and geometric standard deviations (GSD) of the particles for various models.
(T_{in}=1,173 K, T_w=1,173 K, $TiCl_4$=0.5 mole %, O_2=49.75 mole %, carrier gas flow rate=4×10^{-3} m^3/min)

less flattened along the reactor axis. It is, therefore, expected that Model CC-L best follows the limited growth of the primary particles. The geometric standard deviations increase rapidly near the reactor inlet and then decrease after passing through the maximum for all the models. Model C, the coagulation-only model, again gives the highest deviation, while Model CC-L has the lowest of the three. Moreover, in the latter model, the rate of the decrease in the deviation fades out around the reactor exit. It is confirmed that Model CC-L suppresses coagulation, and, as a result, both the average diameter and GSD converge to certain values, respectively, along the reactor axis, respectively.

3. Comparisons of Modeling and Experimental Results

Fig. 6 shows the effect of reaction temperature on the average diameter and geometric standard deviation of the particles for various models. All the models make the average particle size increase with the reaction temperature while the ex-

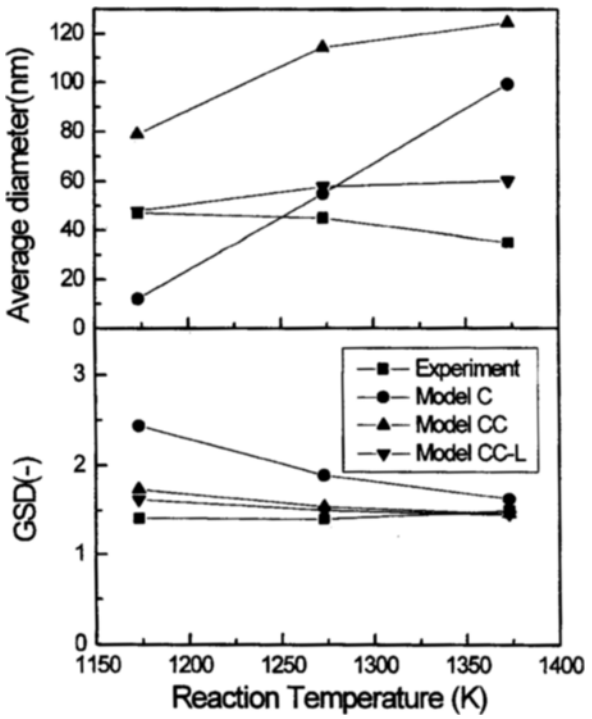

Fig. 6. Effect of reaction temperature on the average diameter and geometric standard deviation (GSD) of the particles for various models.
(T_{in}=reaction temperature, T_w=1,173 K, $TiCl_4$=0.5 mole %, O_2=49.75 mole %, carrier gas flow rate=4×10^{-3} m^3/min)

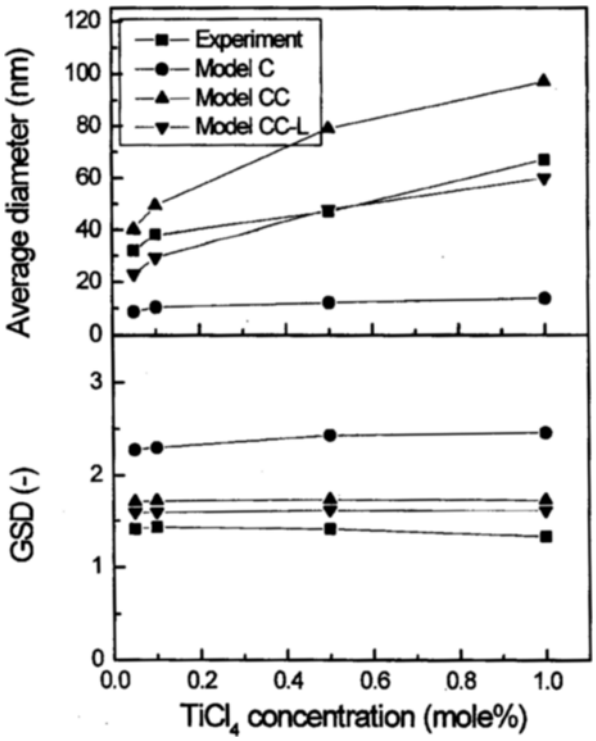

Fig. 7. Effect of $TiCl_4$ concentration on the average diameter and geometric standard deviation (GSD) of the particles for various models.
(T_{in}=1,173 K, T_w=1,173 K, O_2=49.75 mole %, carrier gas flow rate=4×10^{-3} m^3/min)

periment shows the opposite. More monomers are formed by chemical reaction at higher temperature. Thus, in Model C, since the monomers act as nuclei, the coagulation rate among the nuclei increases with the temperature. On the other hand, subsequent coagulation is also enhanced with the temperature due to the temperature effect on the coagulation coefficient [Hinds, 1982]. Therefore, Model C, the coagulation-only model, results in the highest temperature effect on the particle size among the models. The model gives the highest value of the deviation since the coagulation broadens the distribution of particle sizes, as described before. However, in model CC, more monomers produced at higher temperature take part in the formation of more nuclei (dimers) so fewer monomers are available for the subsequent condensational growth of the nuclei. The effect of the reaction temperature on the particle size is, as a result, less pronounced than in Model C. In the figure, Model CC-L, which suppresses the coagulation and, therefore, the temperature effect on the particle size, gives the best agreement with the experimental data among the three. Again for the geometric standard deviations (GSD), the model CC-L gives the best fit to the experimental results. Fig. 7 shows the effect of $TiCl_4$ concentration on the average diameter. The experiment and all the models show the same trend that the average size of the particles increases with the concentration since the latter enhances the production of monomers which are the sources of the particles. The GSD was, however, little affected by $TiCl_4$ concentration for the experiment and all the models. Fig. 8 shows the effect of carrier gas flow rate on the average particle size and GSD. The average size of the particles decreases with the carrier gas

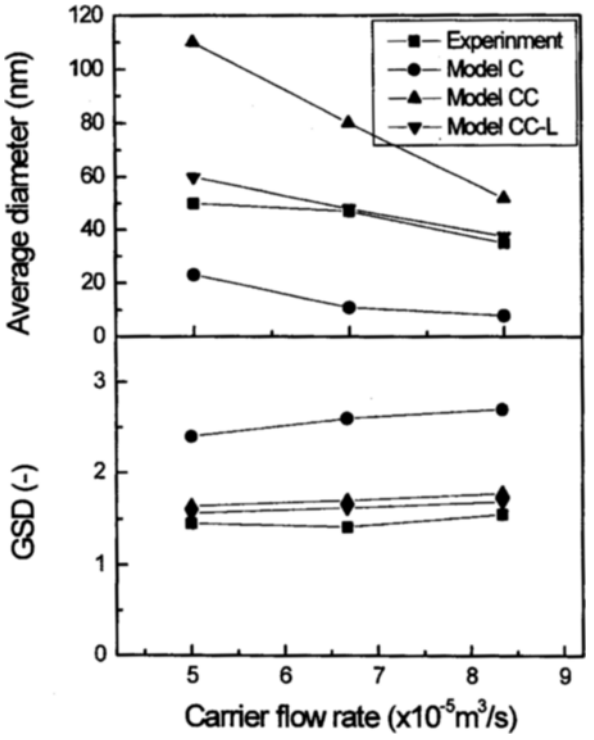

Fig. 8. Effect of carrier gas flow rate on the average diameter and geometric standard deviation (GSD) of the particles for various models.
(T_{in}=1,173 K, T_w=1,173 K, $TiCl_4$=0.5 mole %, O_2=49.75 mole)

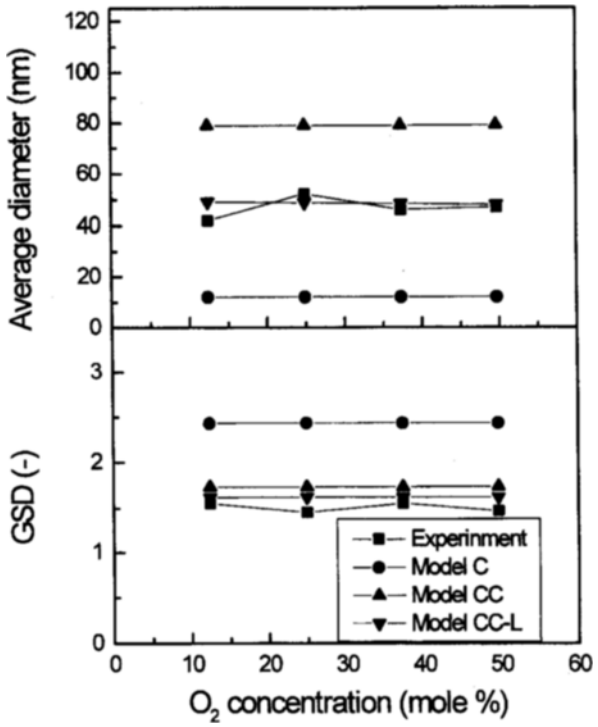

Fig. 9. Effect of the oxygen concentration on the average diameter and geometric standard deviation (GSD) of the particles for various models.
(T_{in}=1,173 K, T_w=1,173 K, $TiCl_4$=0.5 mole %, carrier gas flow rate=4×10^{-3} m^3/min)

flow rate while the deviation slightly increases with it, all due to the reduced residence time in the reactor. The oxygen concentration does not affect either the average diameter or GSD, as shown Fig. 9, which coincides with the experimental trends. This supports the validation of the zeroth order reaction with respect to the oxygen concentration.

Figs. 6 through 9 all show that both the particle sizes and standard deviations calculated from the Model CC-L are closest to those from the experiment. The results come from the consideration of the monomer concentration independently, which enables us to simulate the condensational growth and limit the liquid-like coagulational growth. The meaning of 0.1 as coagulation efficiency is not yet understood and is under investigation. We also had the same efficiency for the preparation of TiO_2 particles by the vapor-phase hydrolysis of titanium tetraisopropoxide, which was carried out at relatively low temperatures (~600 K) [Han, 1996].

CONCLUSION

The growth of ultrafine particles in an aerosol tubular reactor was simulated by moment transformation of the general dynamic equation adding a condensation term and coagulation efficiency. Our model enabled us to investigate the role of monomers in particle growth and to limit the growth of primary particles. The results were compared with the experimental data on the formation of TiO_2 ultrafine particles. By an adjustment of the coagulation efficiency, the average diameter and GSD calculated from the model well fit the data. The model predicted more active growth of particles than did the coagulation-only model. It reflected the roles of highly mobile monomers in condensation, which was not counted in the previous model. Introduction of the adjustable parameter, coagulation efficiency, was very effective in simulating the growth of primary particles, which would not grow infinitely due to the limitation in the rate of sintering.

ACKNOWLEDGEMENT

The authors thank the Chung Ang University for its financial support.

NOMENCLATURE

- b : coagulation coefficient [collisions/m^3s]
- C : $TiCl_4$ mass concentration in the gas [kg/m^3]
- C_0 : $TiCl_4$ mass concentration at the reactor inlet [kg/m^3]
- C_1 : TiO_2 mass concentration in the gas [kg/m^3]
- D : diffusion coefficient of $TiCl_4$ [m^2/s]
- D_1 : diffusion coefficient of TiO_2 monomer [m^2/s]
- D_p : diffusion coefficient of TiO_2 particles [m^2/s]
- k : Boltzmann constant
- k(T) : chemical reaction rate constant at a temperature T [s^{-1}]
- Kn : Knudsen number [-]
- M_k : k-th moment of the particle distribution function
- n : number distribution function of the particles [number/nm]
- r : radial distance in the reactor [m]
- $\vec{r}$: radial displacement vector in the reactor [m]
- R : radius of the reactor [m]
- RXN: reaction rate [kg/m^3s]
- T : temperature [K]
- T_w : temperature at the reactor wall [T]
- T_0 : temperature at the reactor inlet [K]
- x : mass of the particles [kg]
- x_1 : mass of TiO_2 monomer [kg]
- x* : mass of dimer (nuclei) [kg]
- u : axial gas velocity [m/s]
- u_0 : inlet axial gas velocity [m/s]
- v : radial gas velocity [m/s]
- $\vec{V}$: gas velocity vector [m/s]
- $\vec{v}$: particle velocity vector [m/s]
- $\vec{v}_T$: thermophoretic velocity vector of the particle [m/s]
- z : length from the reactor inlet [m]
- z_T : total reactor length [m]
- ϕ : growth rate of particles [kg/s]
- η : coagulation efficiency [-]
- λ : mean free path of the gas [m]
- ρ : gas density [kg/m^3]
- ρ_p : particle density [kg/m^3]
- ν : nucleation rate [number/m^3s]

REFERENCES

Akhtar, M. K., Xiong, Y. and Pratsinis, S. E., "Vapor Synthesis of Titania Powder by Titanium Tetrachloride Oxidation,"

AIChE, **37**, 1561 (1991).

Brock, J. R., "Simulation of Aerosol Dynamics," in Theory of Dispersed Multiflow, Mayer, R. E., ed., Academic Press, New York (1983).

Han, Y. S., "Preparation of Ultrafine TiO_2 and TiO_2/SiO_2 Composite Particles by Vapor-Phase Hydrolysis," M.S. Thesis, Chung Ang University (1996).

Hinds W. C., "Aerosol Technology," John-Wiley & Sons, New York (1983).

Jang, H. D., Lim, Y. W., Jeong J., Kang, T. W. and Shim, G., "Production of Ultrafine Metal Oxide Powder," KIGAM Research Report, KR-95©2-6 (1995).

Kim, S. G. and Brock, J. R., "Growth of Ferromagnetic Particles from Cation Reduction by Borohydride Ions," *J. Colloid & Interf. Sci.*, **116**, 431 (1987).

Landgrebe, J. D. and Pratsinis, S. E., "Discrete Sectional Model for Particulate Production by Gas-Phase Chemical Reaction and Aerosol Coagulation in the Free-Molecular Regime," *J. Colloid & Interf. Sci.*, **139**, 63 (1990).

Lee, K. W., Chen, H. and Gieseke, J. A., "Log-Normally Preserving Size Distribution for Brownian Coagulation in the Free-Molecular Regime," *Aerosol Sci. Technol.*, **3**, 53 (1984).

Pratsinis, S. E. and Kim, K. S., "Particle Coagulation, Diffusion and Thermophoresis in Laminar Tube Flows," *J. Aerosol Sci.*, **20**, 101 (1989).